Structure of the $SnO_2(110)$-(4×1) Surface

Lindsay R. Merte,[1,*] Mathias S. Jørgensen,[2] Katariina Pussi,[3] Johan Gustafson,[1] Mikhail Shipilin,[1] Andreas Schaefer,[1] Chu Zhang,[1] Jonathan Rawle,[4] Chris Nicklin,[4] Geoff Thornton,[5] Robert Lindsay,[6] Bjørk Hammer,[2] and Edvin Lundgren[1]

[1]*Division of Synchrotron Radiation Research, Lund University, 22 100 Lund, Sweden*

[2]*Interdisciplinary Nanoscience Center (iNANO) and Department of Physics and Astronomy, Aarhus University, DK-8000 Aarhus C, Denmark*

[3]*LUT School of Engineering Science, P.O. Box 20, FIN-53851 Lappeenranta, Finland*

[4]*Diamond Light Source, Harwell Science and Innovation Campus, Didcot OX11 0DE, United Kingdom*

[5]*Department of Chemistry and London Centre for Nanotechnology, University College London, London WC1H 0AJ, United Kingdom*

[6]*Corrosion and Protection Centre, School of Materials, University of Manchester, Sackville Street, Manchester M13 9PL, United Kingdom*

(Received 6 January 2017; published 31 August 2017)

Using surface x-ray diffraction (SXRD), quantitative low-energy electron diffraction (LEED), and density-functional theory (DFT) calculations, we have determined the structure of the (4×1) reconstruction formed by sputtering and annealing of the $SnO_2(110)$ surface. We find that the reconstruction consists of an ordered arrangement of Sn_3O_3 clusters bound atop the bulk-terminated $SnO_2(110)$ surface. The model was found by application of a DFT-based evolutionary algorithm with surface compositions based on SXRD, and shows excellent agreement with LEED and with previously published scanning tunneling microscopy measurements. The model proposed previously consisting of in-plane oxygen vacancies is thus shown to be incorrect, and our result suggests instead that Sn(II) species in interstitial positions are the more relevant features of reduced $SnO_2(110)$ surfaces.

DOI: 10.1103/PhysRevLett.119.096102

Tin dioxide (SnO_2) is widely used as the active component of solid-state gas sensors [1], and also sees application in heterogeneous catalysis, where it catalyzes oxidation reactions and enhances the activity of noble metal catalysts [2]. The basis for these applications is the reducibility of the oxide, which allows it to readily and reversibly release oxygen in the presence of reactants such as carbon monoxide or hydrocarbons, and to facilitate adsorption of electronegative species such as O_2 in an anionic state. The changes in conductivity of this *n*-type semiconductor resulting from these surface processes are the basis for the material's gas-sensing characteristics. Because of this, it has long been a goal of fundamental research to characterize the structural, physical, and chemical properties of SnO_2 surfaces. The similarity of the rutile-type SnO_2 crystal structure to that of TiO_2, which has been studied extensively and is considered a "prototypical" reducible metal oxide [3], as well as catalytically active RuO_2 [4], also makes it an interesting material for comparative purposes.

The (110) plane of SnO_2 is the most stable under ambient conditions [5], and efforts to characterize this surface began in the 1980s. The stoichiometric $SnO_2(110)$ surface is reduced readily under vacuum conditions, first releasing oxygen atoms without a detectable change in surface periodicity upon heating above ~400 K. This facile reduction has been attributed to desorption of bridging oxygen (O_{br}) atoms (see Fig. 1), leaving a (1×1) structure [6,7]. Treatment by sputtering and annealing reduces the surface further, and several ordered reconstructions have been observed by low-energy electron diffraction (LEED), including $c(2 \times 2)$, (4×1), and (1×2) phases. The (4×1) phase, to our knowledge first reported by de Frésart *et al.* [8,9], is the only surface structure observed

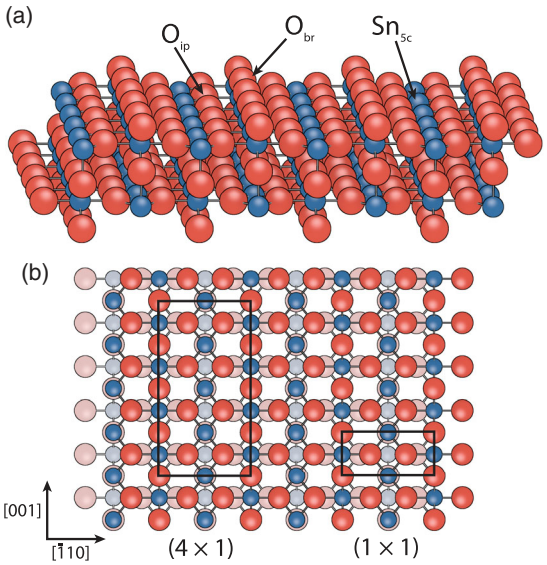

FIG. 1. Side view (a) and top view (b) of the unreconstructed $SnO_2(110)$ surface. The surface exposes twofold coordinated bridging oxygen atoms (O_{br}), threefold coordinated in-plane oxygen atoms (O_{ip}), and fivefold coordinated tin atoms (Sn_{5c}). In (b) the (4×1) and (1×1) unit cells are shown in relation to the surface structure.

which exhibits a high degree of long-range crystalline order [5] and after formation is stable over a broad range of conditions. Nevertheless, despite a number of efforts to determine the structure, based primarily on LEED, scanning tunneling microscopy (STM), and density-functional theory (DFT) calculations, a convincing structural model has remained elusive, preventing well-defined, atomistic studies of the $SnO_2(110)$ surface and, thus, limiting our understanding of the properties of this important material.

An early proposal was that further reduction of the SnO_2 surface after removal of O_{br} atoms should involve oxygen vacancies in the next layer, referred to as the "in-plane" oxygen (O_{ip}, see Fig. 1) [8]. Jones *et al.* imaged the (4×1) surface using STM and observed what appeared to be a lattice of holes, and proposed that the structure consists of an ordered arrangement of such in-plane oxygen vacancies [10]. Quantitative LEED by Atrei *et al.* appeared to confirm this model [11]. Doubts were soon raised about this structure, however. DFT calculations by Oviedo and Gillan found that relaxations predicted for the oxygen vacancy structure were different from those determined by Atrei *et al.*, and that the vacancies should not appear as dark holes in STM images, as had been assumed [12]. Using STM, Batzill *et al.* observed line defects that appeared inconsistent with a structure based on oxygen vacancies; instead, an overlayer chemically similar to SnO was suggested, a possibility that had also been discussed previously by Cox *et al.* [7] and Pang *et al.* [13]. However, subsequent investigations did not lead to likely candidates [14].

In this Letter, we present a model for the (4×1) reconstruction that is consistent with all evidence to date, finally solving this decades-old problem. The first clues leading to the structural model are provided by surface x-ray diffraction (SXRD), a technique which had not previously been applied to this surface. The detailed structure is the result of a DFT-based search using an evolutionary algorithm [15]. Confirmation of this structure comes from comparison with a more extended set of LEED $I(V)$ measurements than that reported by Atrei *et al.*, which is also found to be inconsistent with the vacancy model. The structure furthermore is predicted to yield STM images showing a lattice of holes, similar to those reported previously [5,10,13,16].

Figure 2 shows the results of SXRD measurements of a $SnO_2(110)$ single crystal, acquired on beam line I07 at the Diamond Light Source [17]. The crystal was prepared following previous studies [2] by Ar^+ sputtering and annealing in ultrahigh vacuum (UHV) at ~1000–1200 K, after which it exhibited a (4×1) structure as evidenced by *in situ* LEED measurements (for details of sample preparation and characterization, see the Supplemental Material [18]). SXRD measurements were acquired in the attached analysis chamber, also under UHV conditions. In total, 45 in-plane structure factors were measured from rocking curves at out-of-plane reciprocal space coordinate $L = 0.5$, reduced by averaging to 17 inequivalent rods. The results are plotted in

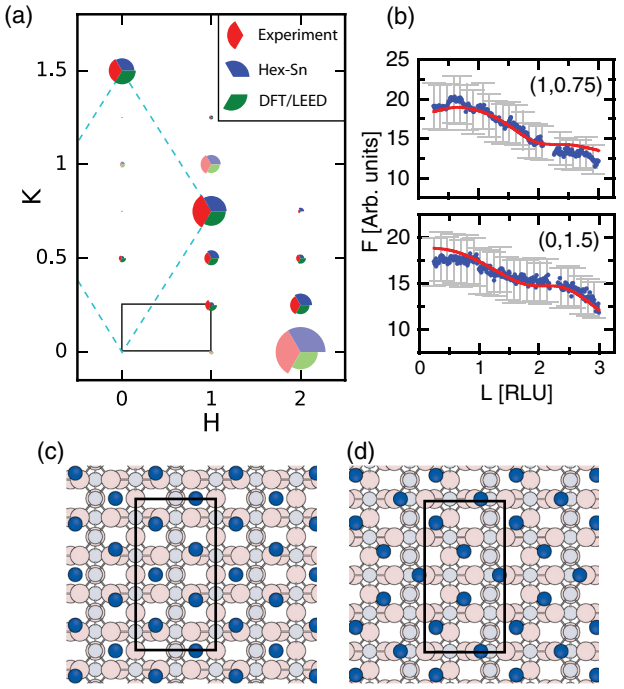

FIG. 2. (a) Measured and calculated in-plane SXRD structure factors at $L = 0.5$. The dashed line shows the reflexes corresponding to the quasihexagonal arrangement adopted by the Sn, depicted in (c). (b) Out-of-plane structure factors measured for the two strongest superstructure rods (blue points). Calculated structure factors are plotted for the structure determined by DFT + LEED (red lines). (c) Hexagonal Sn monolayer suggested by the dominant diffraction rods at (1,0.75) and (0,1.5). (d) Distorted hexagonal arrangement found by least-squares fit to the experimental data.

Fig. 2(a). Consistent with LEED measurements, alternating rods along $H = 0$ [i.e., at (0,0.25), (0,0.75), etc.], are absent, indicating the presence of a glide plane in the [001] direction. The most intense of the fractional-order rods, dominating the surface diffraction pattern, is that at (1,0.75), while the second-most-intense rod is found at (0,1.5). The other measured rods are significantly weaker. Out-of-plane scans of these dominant rods are plotted in Fig. 2(b) and show relatively smooth profiles with only subtle oscillations, indicating that the phase essentially consists of a monolayer structure.

The observation of these dominant rods suggests, as a first approximation, a structure based on a hexagonal layer of Sn ions, arranged such that a $(3 \times 1)/(4 \times 1)$ coincidence is formed, depicted in Fig. 2(c). Restricting the symmetry to the group $p2mg$ and allowing relaxation of the atoms in a least-squares fit to the diffraction data (computed using the ROD software package [31]), a distorted hexagonal structure is found [Fig. 2(d)] that is able to reproduce the experimental structure factors well. Because of the large difference in x-ray form factor between Sn and O, the addition of oxygen atoms in different configurations to the trial models had only modest effects on the calculated diffraction patterns, precluding a complete structure determination on the basis of SXRD data alone.

To identify an overlayer structure that can reproduce the diffraction data and is plausible energetically, we performed a systematic DFT search using an evolutionary algorithm (EA) [15,18], taking as a starting point the findings of SXRD. Randomized starting configurations were constructed based on a slab consisting of one complete $SnO_2(110)$ trilayer and an overlayer consisting of 6 tin atoms, plus 2, 4, 6, or 8 oxygen atoms, in a (4×1) unit cell. The O_{br} atoms of the trilayer were included in the group of randomized atoms to allow for reduction of the slab. Four EA runs were performed for each stoichiometry, during which a total of 6125 unique structures were tested. The EA run was stopped when no lower-energy structure was found after several hundred iterations. The lowest-energy structures were then refined further using a thicker slab consisting of three SnO_2 trilayers, with atoms in the bottommost layer frozen in bulk positions.

Of the four stoichiometries tested, only the Sn_6O_6 composition (O_{br} are excluded, as inclusion of these would give a composition of Sn_6O_{10}) yielded a structure with symmetry properties consistent with experiments; this structure, shown in Figs. 3(a) and 3(b), was found as the global minimum energy configuration in each of the four EA runs. The structure is composed of two equivalent Sn_3 clusters per unit cell, with each Sn atom bound to the surface

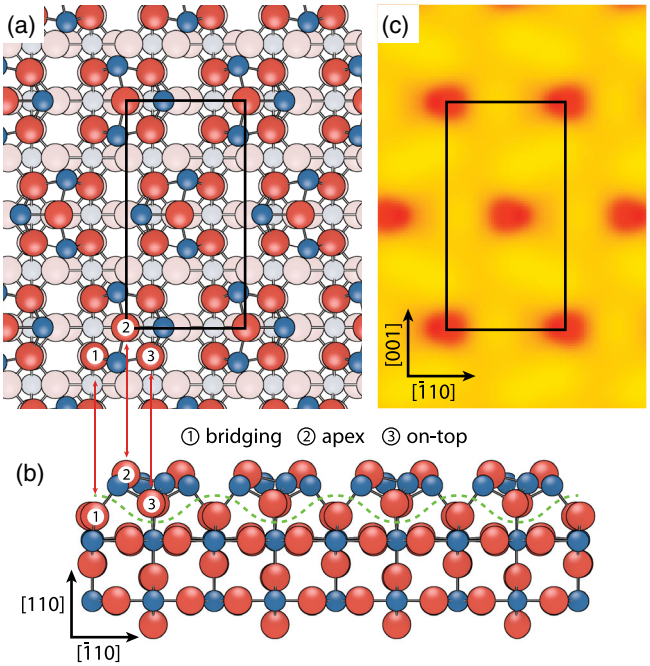

FIG. 3. Structure of the (4×1) reconstruction as determined from DFT calculations: (a) top view, (b) side view. The three different types of oxygen atoms bound to overlayer Sn atoms are labeled. The dashed line in (b) indicates the division between substrate and overlayer atoms for the purpose of calculating stoichiometry. (c) Simulated STM image based on the Tersoff-Hamann approximation, calculated for a bias of +1 V at a height of 3.7 Å above the outermost Sn atoms. The unit cell marked corresponds to that shown in (a).

via on-top and bridging oxygen atoms, and an additional "apex" O atom occupying the threefold hollow site atop the Sn trimer. Each Sn atom and each O atom in the overlayer is bound to three O or Sn atoms, respectively. The Sn—O bond lengths are in the range of 2.1–2.2 Å, and the Sn atoms are nearly coplanar, at heights of 3.0–3.2 Å above the topmost SnO_2 trilayer. The outermost atoms are the O at the centers of the trimers, about 0.6 Å above the Sn. The distance between Sn atoms in neighboring trimers is 3.8 Å, indicating minimal chemical bonding between clusters.

Considering only geometric factors, this structure would appear difficult to reconcile with published STM images showing a hexagonal lattice of holes. These holes were previously interpreted either as oxygen vacancies [10] or as empty pockets in an overlayer structure [5]. Nevertheless, the simulated STM image of the Sn_6O_6 structure, calculated for positive sample bias based on the Tersoff-Hamann approximation [32], strongly resembles the published images [Fig. 3(c)]. The "holes" observed in the simulated image in fact result from a local reduction in the unoccupied local density of states (LDOS) above the outermost oxygen atoms. Analysis of the calculated electronic structure [18] shows that the LDOS above the Sn_6O_6 surface is dominated by Sn $5p$ states, so that the structure exhibits "inverted" STM contrast. Such effects are well known for metal oxides, the most prominent example being rutile $TiO_2(110)$-(1×1), which exhibits bright rows above Ti atoms in STM images at positive bias, instead of the higher-lying bridging oxygens [33].

Additional support for the proposed (4×1) model comes from quantitative LEED measurements. Using a $SnO_2(110)$ single crystal prepared similarly as in the SXRD experiment, we collected a set of $I(V)$ measurements for 15 inequivalent LEED beams, plotted in Fig. 4. To fit the data to theoretical LEED intensities given by multiple-scattering calculations, we used the atomic coordinates for the Sn_6O_6 structure from the DFT calculation (scaled to the experimental lattice parameter of SnO_2) as initial values and allowed relaxation of the z coordinates only. The best-fit structure, which differs from the DFT result by only a small (< 0.1 Å) inward relaxation of the 6 Sn atoms, gives a Pendry reliability factor (R_P) [34] of 0.16, indicating that the model describes the experimental data well. Using the resulting model based on DFT and LEED, we also simulated the in-plane and out-of-plane SXRD structure factors, which are plotted in Figs. 2(a) and 2(b). This also shows good agreement with experiment, including the subtle undulations in out-of-plane structure factor with L, the period of which reflects primarily the (~3 Å) height of the plane of Sn atoms in the overlayer above the uppermost Sn-containing plane of the substrate.

The SXRD and LEED measurements also allow us to safely exclude the in-plane vacancy model found by Atrei *et al.* [11]. This model does not produce a surface x-ray diffraction pattern dominated by the (1,0.75) rod [18], and

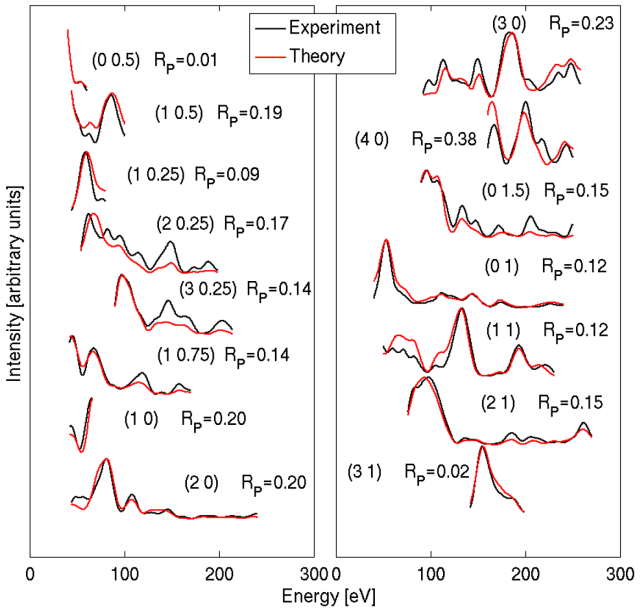

FIG. 4. LEED $I(V)$ measurements for $SnO_2(110)$-(4×1). The Pendry reliability factors for each beam are given. The cumulative R_P was 0.16.

LEED $I(V)$ fits yield an unacceptably large R_P of 0.6 (using a subset of our data comparable to that used by Atrei *et al.*, we obtain an R_P of 0.3, consistent with their results). The "interstitial" model suggested by Batzill *et al.* [5] as an analog of the (1×2) structure observed on $TiO_2(110)$ likewise produces a surface x-ray diffraction pattern qualitatively different from the observed one, and gives an R_P of 0.42 in LEED. First-principles thermodynamics calculations including these two structures as well as the global minimum structures found by the EA optimization also show that the Atrei and Batzill models are not expected to be stable under any conditions, consistent with previous calculations by Ágoston and Albe [14]. This is demonstrated in Fig. 3 in the Supplemental Material [18], which displays plots of surface energy as a function of oxygen chemical potential [Fig. 3(a)] and the surface phase diagram as a function of oxygen pressure and temperature [Fig. 3(b)]. Furthermore, the Sn_6O_6 model is found to be the most stable surface phase for oxygen chemical potentials between ~0.8 and 1.2 eV, which at ambient O_2 pressure corresponds to a range of stability between ~600–900 K.

The structure found for the (4×1) reconstruction, comprising essentially isolated Sn_3O_3 (or Sn_3O_5) clusters with Sn in trigonal pyramidal coordination, is different from the reconstructions observed for reduced $TiO_2(110)$, made up of continuous chains of fourfold coordinated Ti oriented along the [001] direction [35,36]. Trigonal pyramidal coordination, on the other hand, is common in tin(II) compounds, with the asymmetry typically attributed to a nonbonding lone electron pair on Sn [37]; very similar coordination was observed for tin(II) ions at the reduced $SnO_2(011)$ surface [38]. Assigning bridging O atoms formally to the SnO_2 substrate and the rest to the overlayer, the phase can be considered to consist of tin(II) oxide clusters atop the tin(IV) oxide substrate. Presumably this favorable coordination state is responsible for the stability and relative inertness of the (4×1) phase, which was found, counterintuitively, to be less reactive to several adsorbates than less-reduced surfaces prepared by heating [39–41]. Consistent with the structural similarity, this inertness is analogous to that observed for reduced $SnO_2(011)$ [38]. It bears mentioning that an early proposal for the structure of the (4×1) reconstruction was that of an SnO overlayer, and the quasihexagonal Sn sublattice we observe is in fact similar to that of the litharge SnO(101) plane discussed by Cox *et al.* [7]. Considering the difference in bonding configurations and the fact that the (101) is not a cleavage plane of SnO, however, we consider the resemblance largely coincidental.

Having determined the structure of the (4×1) phase, we can begin to address the question of its relevance in technical applications. So far, the phase has only been observed following preparation by sputtering under UHV conditions, suggesting that it arises only due to the exceptionally strong enrichment of tin caused by the sputtering process [2], so that its appearance under catalytic or gas-sensing conditions would appear unlikely. The structure we have found, however, does not exhibit an unusually high Sn:O ratio and is predicted by DFT to be stable over a rather wide range of conditions (see Fig. 3 in the Supplemental Material [18]). These findings, together with the observed thermal and chemical stability of the structure once formed, suggest that kinetic limitations may be responsible for the fact that the (4×1) phase has not been observed upon heating of thoroughly oxidized single crystal samples in UHV. For nanostructured, composite, or otherwise different SnO_2 materials, and for materials exposed to elevated gas pressures or electrochemical environments, such limitations should be less significant, and the formation of the reconstruction should be anticipated under mildly reducing conditions. We note further that the Sn_3O_3 clusters that form the basic unit of the reconstruction are discrete species that can, in principle, exist in other ordered or disordered arrangements or as isolated minority species on the surfaces of SnO_2 crystallites. The local atomic arrangement should thus be considered the defining characteristic of this phase, rather than its long-range periodicity.

Despite earlier doubts about the (4×1) model based on O_{ip} vacancies, the idea that such vacancies, alongside more easily formed O_{br} vacancies, play an essential role in SnO_2 surface chemistry has been an enduring one (see, for example, Refs. [42,43]). Our results do not entirely refute this hypothesis, there being a number of ordered and disordered surface phases whose structures are still unknown. However, we can find no direct experimental evidence for O_{ip} vacancies in studies of reduced $SnO_2(110)$ surfaces in the published literature, and the strong evidence

we present for the formation of SnO-type structures should be taken as an indication that such species, based on tin atoms in "interstitial" positions, are more common features of reduced $SnO_2(110)$.

Considering the importance of SnO_2 surface conductivity in gas-sensing applications, it is a natural question whether upon formation of the reduced (4×1) phase the surface becomes metallic. To address this, we have evaluated the calculated density of states (DOS) of the upper layers in our structures (see Fig. 5 in the Supplemental Material [18]). This shows that, despite the deficiency of O in the Sn_3O_3 clusters, this surface remains insulating, exposing a small band gap. This rationalizes the photoelectron spectroscopy measurements by Batzill *et al.* [44], who found weak emission from the bulk band-gap region for the (4×1) structure when using surface-sensitive photon energies. Subsequent oxidizing and annealing cycles showed more states in the bulk band-gap region, though these were presumably caused by kinetically trapped oxygen vacancies in the near-surface region. Once fully oxidized, the (1×1) structures were observed to exhibit a small band gap and to have a valence DOS very similar to that of the (4×1), both in agreement with our results.

To conclude, the (4×1) phase, as the first to be solved with confidence, can now serve as a useful model for fundamental studies of $SnO_2(110)$ surface chemistry and a basis for further studies that should help resolve the complex behavior of the surface under different conditions.

We gratefully acknowledge support from the Swedish Research Council by the Röntgen-Ångström Cluster "Catalysis on the atomic scale" (Project No. 349-2011-6491). This work was supported by the Academy of Finland under Grant No. 277829 and the Danish Research Council under Grant No. 0602-02566B. LEED calculations were done at CSC-IT Center for Science, Finland.

*lindsay.merte@sljus.lu.se

[1] M. Batzill and U. Diebold, Phys. Chem. Chem. Phys. **9**, 2307 (2007).
[2] M. Batzill and U. Diebold, Prog. Surf. Sci. **79**, 47 (2005).
[3] U. Diebold, Surf. Sci. Rep. **48**, 53 (2003).
[4] H. Over, Y. D. Kim, A. P. Seitsonen, S. Wendt, E. Lundgren, M. Schmid, P. Varga, A. Morgante, and G. Ertl, Science **287**, 1474 (2000).
[5] M. Batzill, K. Katsiev, and U. Diebold, Surf. Sci. **529**, 295 (2003).
[6] D. F. Cox, T. B. Fryberger, and S. Semancik, Phys. Rev. B **38**, 2072 (1988).
[7] D. F. Cox, T. B. Fryberger, and S. Semancik, Surf. Sci. **224**, 121 (1989).
[8] E. de Frésart, J. Darville, and J. M. Gilles, Solid State Commun. **37**, 13 (1981).
[9] E. de Frésart, J. Darville, and J. M. Gilles, Appl. Surf. Sci. **11–12**, 637 (1982).
[10] F. H. Jones, R. Dixon, J. S. Foord, R. G. Egdell, and J. B. Pethica, Surf. Sci. **376**, 367 (1997).
[11] A. Atrei, E. Zanazzi, U. Bardi, and G. Rovida, Surf. Sci. **475**, L223 (2001).
[12] J. Oviedo and M. J. Gillan, Surf. Sci. **513**, 26 (2002).
[13] C. L. Pang, S. A. Haycock, H. Raza, P. J. Møller, and G. Thornton, Phys. Rev. B **62**, R7775 (2000).
[14] P. Ágoston and K. Albe, Surf. Sci. **605**, 714 (2011).
[15] L. B. Vilhelmsen and B. Hammer, J. Chem. Phys. **141**, 044711 (2014).
[16] M. Sinner-Hettenback, M. Göthelid, J. Weissenrieder, H. von Schenck, T. Weiss, N. Barsan, and U. Weimar, Surf. Sci. **477**, 50 (2001).
[17] C. Nicklin, T. Arnold, J. Rawle, and A. Warne, J. Synchrotron Radiat. **23**, 1245 (2016).
[18] See Supplemental Material at http://link.aps.org/supplemental/10.1103/PhysRevLett.119.096102 for experimental and computational details, atomic coordinates for the structure, and additional supporting data, as well as Refs. [19–30].
[19] M. Batzill, Sensors **6**, 1345 (2006).
[20] J. Drnec, T. Zhou, S. Pintea, W. Onderwaater, E. Vlieg, G. Renaud, and R. Felici, J. Appl. Crystallogr. **47**, 365 (2013).
[21] E. Vlieg, J. Appl. Crystallogr. **30**, 532 (1997).
[22] ANA-ROD, European Synchrotron Radiation Facility, http://www.esrf.eu/computing/scientific/joint_projects/ANA-ROD.
[23] M. A. Van Hove, W. Moritz, H. Over, P. J. Rous, A. Wander, A. Barbieri, N. Materer, U. Starke, and G. A. Somorjai, Surf. Sci. Rep. **19**, 191 (1993).
[24] A. Barbieri and M. A. Van Hove (private communication).
[25] L. B. Vilhelmsen and B. Hammer, Phys. Rev. Lett. **108**, 126101 (2012).
[26] S. R. Bahn and K. W. Jacobsen, Comput. Sci. Eng. **4**, 56 (2002).
[27] D. M. Deaven and K. M. Ho, Phys. Rev. Lett. **75**, 288 (1995).
[28] J. J. Mortensen, L. B. Hansen, and K. W. Jacobsen, Phys. Rev. B **71**, 035109 (2005).
[29] J. P. Perdew, K. Burke, and M. Ernzerhof, Phys. Rev. Lett. **77**, 3865 (1996).
[30] K. Reuter and M. Scheffler, Phys. Rev. B **65**, 035406 (2001).
[31] E. Vlieg, J. Appl. Crystallogr. **33**, 401 (2000).
[32] J. Tersoff and D. R. Hamann, Phys. Rev. Lett. **50**, 1998 (1983).
[33] U. Diebold, J. F. Anderson, K.-O. Ng, and D. Vanderbilt, Phys. Rev. Lett. **77**, 1322 (1996).
[34] J. B. Pendry, J. Phys. C **13**, 937 (1980).
[35] Q. Wang, A. R. Oganov, Q. Zhu, and X.-F. Zhou, Phys. Rev. Lett. **113**, 266101 (2014).
[36] I. Mochizuki, H. Ariga, Y. Fukaya, K. Wada, M. Maekawa, A. Kawasuso, T. Shidara, K. Asakura, and T. Hyodo, Phys. Chem. Chem. Phys. **18**, 7085 (2016).
[37] M. Veith and O. Recktenwald, in *Organotin Compounds* (Springer, Berlin, Heidelberg, 1982), pp. 1–55.
[38] M. Batzill, K. Katsiev, J. M. Burst, Y. Losovyj, W. Bergermayer, I. Tanaka, and U. Diebold, J. Phys. Chem. Solids **67**, 1923 (2006).

[39] V. A. Gercher, D. F. Cox, and J.-M. Themlin, Surf. Sci. **306**, 279 (1994).
[40] V. A. Gercher and D. F. Cox, Surf. Sci. **322**, 177 (1995).
[41] M. W. Abee and D. F. Cox, Surf. Sci. **520**, 65 (2002).
[42] X. Wang, H. Qin, Y. Chen, and J. Hu, J. Phys. Chem. C **118**, 28548 (2014).
[43] V. Bonu, A. Das, A. K. Prasad, N. G. Krishna, S. Dhara, and A. K. Tyagi, Appl. Phys. Lett. **105**, 243102 (2014).
[44] M. Batzill, K. Katsiev, J. M. Burst, U. Diebold, A. M. Chaka, and B. Delley, Phys. Rev. B **72**, 165414 (2005).